Chemical Engineering Science 137 (2015) 852–861

Contents lists available at ScienceDirect

Chemical Engineering Science

journal homepage: www.elsevier.com/locate/ces

Discrete element method prediction of particle curtain properties

R.J. Goetsch, J.D. Regele *

Department of Aerospace Engineering, Iowa State University, Ames, IA 50011, USA

HIGHLIGHTS

- The discrete element method is used to predict the properties of a particle curtain.
- Model is validated through comparison with granular channel flow experiment.
- Estimate velocity and volume fraction profiles in particle curtain.
- Volume fraction in particle curtain is not uniform as previously expected.

GRAPHICAL ABSTRACT

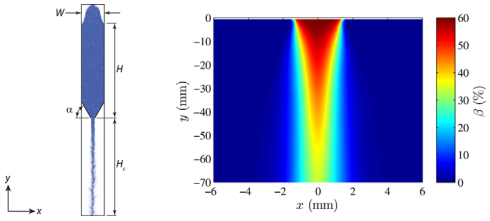

ARTICLE INFO

Article history:
Received 3 May 2015
Received in revised form
21 July 2015
Accepted 29 July 2015
Available online 6 August 2015

Keywords:
Discrete element method
Granular channel flow
Granular temperature
Particle curtain
Hopper flow

ABSTRACT

The discrete element method (DEM) is used to predict the properties of a particle curtain created by the three-dimensional granular flow through a hopper constricted by a slit opening. The profiles of the mean and fluctuation velocity components and solid volume fraction within the particle curtain are estimated. The model is validated against experimental measurements of the mean and fluctuation velocity profiles in a granular channel flow. Good agreement is observed between the experimental channel flow measurements and our DEM simulations. The approach is extended to model the behavior of the particle curtain after it exits the hopper. The model predictions suggest that the volume fraction is not uniform across the curtain as expected from experimental results.

© 2015 Elsevier Ltd. All rights reserved.

1. Introduction

Multiphase particle-laden flows occur in a wide variety of phenomena. Some, such as fluidized bed reactors, have very important industrial applications. For this reason, these types of flows have been actively studied for decades. There has been success in modeling these flows when the solid phase is in either the dilute (Drew, 1983; Magnaudet and Eames, 2000; Crowe et al., 2012) or densely packed (Baer and Nunziato, 1986; Powers et al., 1990) regimes. However, the modeling of compressible flows when the solid phase has a volume fraction between these extremes has lagged behind (Wagner et al., 2012). Additionally, this intermediate regime of multiphase flows has seen relatively little experimental investigation due to the difficulties in isolating and measuring the high solid volume fraction regions.

A recent experiment has been developed that successfully isolates this multiphase flow regime by investigating the interaction between a shock wave and a dense non-compacted particle curtain (Wagner et al., 2012). The particle curtain used in this experiment is generated by the granular flow of glass beads through a hopper with a slit opening. Schlieren images in conjunction with pressure measurements are used to characterize the flow features. However, due to the high volume fraction of particles within the particle curtain, the flow features are not directly observable. Regele et al. (2014) performed numerical simulations of a shock wave passing through a cloud of cylinders that are fixed in place to develop a better sense of how the flow unsteadiness behaves inside of the curtain and immediately downstream. However, it is still unclear how the particle motion and interaction between the fluid and moving particles affect the flow dynamics during this interaction. Numerical simulation of this interaction is a logical next step

* Corresponding author.
E-mail address: jregele@iastate.edu (J.D. Regele).

http://dx.doi.org/10.1016/j.ces.2015.07.034
0009-2509/© 2015 Elsevier Ltd. All rights reserved.

towards understanding this behavior, but details about the particle curtain flow properties such as the mean and fluctuation velocities as well as a detailed account of the spatial particle distribution are not contained in Wagner et al. (2012).

Hopper flows similar to that in Wagner et al. (2012) have been the focus of many experimental investigations due to their importance in many industrial processes. Some recent examples of such experimental work can be found in Sielamowicz et al. (2006) and Li et al. (2004). The focus of these experiments is on characterizing the dependence of the velocity field and discharge rate on the particle properties and hopper geometry. However, the literature that details the flow conditions downstream of the hopper exit is still missing.

Detailed information about the flow conditions downstream of the hopper exit may be found using numerical simulations. However, the flow of granular materials has been notoriously difficult to model and predict. This is partly due to the wide range of behaviors that granular flows can exhibit. They are known to exhibit the behavior of a solid, liquid or gas depending on the amount of external energy supplied to the system (Olivier and François, 2002; Jop et al., 2006). Additionally, accurate experimental measurements of opaque granular materials have many difficulties, which in part has lead to a significant lack of experimental information (Savage, 1979; Moka and Nott, 2005; Shäfer et al., 1996). This wide range of behaviors and lack of information has complicated the efforts in obtaining a universal continuum model (Choi et al., 2004; Shäfer et al., 1996). For these reasons, much of the research in this field has relied on numerical simulations using a Lagrangian approach, where the trajectories of individual grains within a granular media are obtained. In many ways these numerical simulations have lead experimental work in obtaining the detailed measurements needed for the development of models (Shäfer et al., 1996; Hirshfeld et al., 1997).

Perhaps the most widely used method used in these numerical studies is the discrete element method (DEM), which was originally formulated by Cundall and Strack (1979). In this method, the motion of individual grains is obtained through numerical integration of Newton's second law. The grains are allowed to slightly overlap, and the collisional forces are modeled as a function of the overlap distance. The DEM has been successfully used to better understand granular flows in a wide variety of applications, as recently summarized by Zhu et al. (2008).

The DEM has been useful in the study of hopper flows. Simulations have characterized the effects of particle properties and hopper geometry on the discharge properties of hoppers (Anand et al., 2008; Ketterhagen et al., 2007; Li et al., 2004). However, these studies, like others in the literature, focus on the region within the hopper, leaving the properties of the particle curtain that is formed after the particles exit the hopper uninvestigated. Thus, the primary objective of this work is to use DEM simulations to characterize the particle flow conditions downstream of the hopper exit. The conditions used in Wagner et al. (2012) will be used so that quantitative comparisons can be made.

In order to have confidence in the results from a numerical simulation, we first look to validate the model with detailed experimental measurements. While there is little to no experimental work studying the properties of a particle curtain similar to that used in Wagner et al. (2012), there are a few classes of basic granular flows that have been thoroughly studied. These include plane shear, annular shear, vertical channel flows, inclined plane, heap flow, and rotating drums (MiDi, 2004). The flow that is most similar to the particle curtain of interest is the vertical channel flow, as this flow exists in the feed hopper region. In an experiment by Natarajan et al. (1995), the profiles of the mean and fluctuation velocities within a channel were measured through optical particle tracking. These results are used as a benchmark to show that the model is able to predict the properties of the particle curtain below the channel.

The paper is organized as follows. First, the numerical approach will be discussed in Section 2 followed by a validation of the model in Section 3. The prediction of the particle curtain properties will then be discussed in Section 4. Finally, a summary and final conclusions will be included in Section 5.

2. Numerical model

2.1. Equations of motion

The motion of each individual grain in a granular medium is fully described by Newton's second law for linear and angular motion

$$m_i \frac{d^2 \boldsymbol{r}_i}{dt^2} = \boldsymbol{F_i} \tag{1}$$

$$I_i \frac{d\boldsymbol{\omega}_i}{dt} = \boldsymbol{T}_i, \tag{2}$$

where the subscript i represents the particle index, m is the mass, $\boldsymbol{r}$ is the position vector, t is the time, $\boldsymbol{F}$ is the total external force, I is the moment of inertia, $\boldsymbol{\omega}$ is the angular velocity vector, and $\boldsymbol{T}$ is the total external torque acting on the particle.

The external force $\boldsymbol{F}_i$ is commonly broken into components that are each modeled separately

$$\boldsymbol{F}_i = \sum_{j,\, j \neq i} (\boldsymbol{F}_{n,ji} + \boldsymbol{F}_{t,ji}) + \boldsymbol{F}_{ext,i}, \tag{3}$$

where $\boldsymbol{F}_{n,ji}$ and $\boldsymbol{F}_{t,ji}$ are the normal and tangential components, respectively, of the contact force acting on particle i due to particle j. The term $\boldsymbol{F}_{ext,i}$ represents any additional external forces not caused by particle–particle contact including gravitational forces, contact with walls, and fluid forces. The torque on the particle i is related to the force acting on it through

$$\boldsymbol{T}_i = \sum_{j,\, j \neq i} (R_i \boldsymbol{n}_{ji} \times \boldsymbol{F}_{t,ji}), \tag{4}$$

where $\boldsymbol{n}_{ji}$ is the normal unit vector that points from the center of particle i to the center of particle j and R_i is the radius of particle i.

2.2. Collision model

The first part of this section focuses on the normal component, $\boldsymbol{F}_{n,ji}$, of the contact force between two spheres. One of the most simple and widely used models is a linear-spring and dashpot. In this model, the normal contact force is given by

$$\boldsymbol{F}_{n,ji} = -k_n \delta_{n,ji} \boldsymbol{n}_{ji} - \eta_n \boldsymbol{v}_{n,ji}, \tag{5}$$

where k_n is the normal spring stiffness and $\boldsymbol{v}_{n,ji}$ is the normal component of the velocity of particle j relative to particle i. The normal component of the overlap $\delta_{n,ji}$, unit normal vector, and velocity of the surface of particle j relative to i at the point of contact are

$$\delta_{n,ji} = (R_i + R_j) - |\boldsymbol{r}_j - \boldsymbol{r}_i| \tag{6}$$

$$\boldsymbol{n}_{ji} = \frac{\boldsymbol{r}_j - \boldsymbol{r}_i}{|\boldsymbol{r}_j - \boldsymbol{r}_i|} \tag{7}$$

$$\boldsymbol{v}_{ji} = (\boldsymbol{v}_j - \boldsymbol{v}_i) + (R_i \boldsymbol{\omega}_i + R_j \boldsymbol{\omega}_j) \times \boldsymbol{n}_{ji}, \tag{8}$$

respectively, where the normal component of the relative velocity is

$$\boldsymbol{v}_{n,ji} = (\boldsymbol{v}_{ji} \cdot \boldsymbol{n}_{ji}) \boldsymbol{n}_{ji}. \tag{9}$$

The damping coefficient η_n is related to the restitution coefficient e (Hu et al., 2011; van der Hoef et al., 2006; Deen et al., 2007)

$$\eta_n = \frac{-2\ln e\sqrt{m^* k_n}}{\sqrt{\pi^2+\ln^2 e}} \quad (e \neq 0), \tag{10}$$

where it can take values in the range $0 < e \leq 1$ and m^* is

$$m^* = \left(\frac{1}{m_i}+\frac{1}{m_j}\right)^{-1}. \tag{11}$$

We now look at the tangential component of the contact force $\boldsymbol{F}_{t,ji}$. An analogous linear-spring and damper model is commonly used. However, in the tangential direction this force is limited by a Coulomb-type sliding friction force

$$\boldsymbol{F}_{t,ji} = \begin{cases} -k_t\boldsymbol{\delta}_t - \eta_t \boldsymbol{v}_{t,ji}, & |\boldsymbol{F}_{t,ji}| \leq \mu |\boldsymbol{F}_{n,ji}| \\ -\mu_f |\boldsymbol{F}_{n,ji}| \boldsymbol{t}_{ji}, & |\boldsymbol{F}_{t,ji}| > \mu |\boldsymbol{F}_{n,ji}|, \end{cases} \tag{12}$$

where k_t, $\boldsymbol{\delta}_t$, η_t, and μ are the tangential stiffness, relative displacement, damping coefficient, and coefficient of friction, respectively. The tangential relative velocity and unit vector are found using

$$\boldsymbol{v}_{t,ji} = \boldsymbol{v}_{ji} - \boldsymbol{v}_{n,ji} \tag{13}$$

$$\boldsymbol{t}_{ji} = \frac{\boldsymbol{v}_{t,ji}}{|\boldsymbol{v}_{t,ji}|}. \tag{14}$$

The tangential relative displacement in 2-D is calculated by integrating the tangential velocity

$$\boldsymbol{\delta}_t = \boldsymbol{\delta}_{t_0} + \int_{t_0}^{t} \boldsymbol{v}_{t,ji}(t')\, dt'. \tag{15}$$

However, this formula requires storing δ for all pairs of particles that are in contact and adds significant computational expense. Additionally, in 3-D simulations, the rotation of the contact plane requires coordinate transformations between time steps (van der Hoef et al., 2006).

An alternative friction model that eliminates the need to calculate Eq. (15) is the static friction model. The friction force is represented simply as the static friction component of the above equation

$$\boldsymbol{F}_{t,ji} = -\mu_f |\boldsymbol{F}_{n,ji}| \boldsymbol{t}_{ji}. \tag{16}$$

As discussed in Capecelatro and Desjardins (2013), this simplified model is a good compromise between accuracy and computational cost for granular flows dominated by sustained contact. This is further investigated in Appendix A.

The same equations used to compute contact forces between particles are also used to compute the particle–wall contact forces. These contact forces occur at non-periodic system boundaries and the plane segments that constrict the channel to a slit opening at the bottom. In these collisions, the closest point to the center of the particle that lies on the wall is treated as particle j with $R_j = 0$ and $m_j = \infty$. In effect, this treats a wall as a point particle with infinite mass. This allows the calculation of $\boldsymbol{F}_n$ and $\boldsymbol{F}_t$ using the same models as for particle–particle collisions.

2.3. Time integration and parallelization

The equations of motion of the system of particles described in Section 2.1 above are a coupled system of ordinary differential equations. The initial conditions of the particles are known, therefore this represents an initial value problem where the solution can be marched through time. In this work, a second order Runge–Kutta method is used.

Because of the stiff nature of the equations of motion, a very small time step is needed to properly resolve the collisions and ensure conservation of energy. It is common practice to restrict the time step by forcing N steps to occur within the duration of a collision. The exact solution to the equations of motion shows that the collision duration is (Capecelatro and Desjardins, 2013)

$$\tau = \sqrt{[\pi^2 + \ln(e)^2]\frac{m^*}{k_n}}. \tag{17}$$

The maximum allowable time step is then $dt_{\max} = \tau/N$. When simulating a system of non-uniform diameter particles, the smallest value of $dt_{\max}$ for all pairs of particles is chosen to ensure at least N time steps are taken during each collision. In previous work, N values of 10–100 have been used (Shäfer et al., 1996; Capecelatro and Desjardins, 2013; Cleary and Sawley, 2002). In this work, the time step size is chosen such that $N \geq 50$ is enforced unless otherwise specified.

In order to avoid $O(N_p^2)$ operations required by Eq. (3), where N_p is the total number of particles, a linked cell algorithm is used (Cleary and Sawley, 2002; Capecelatro and Desjardins, 2013; Pöschel and Schwager, 2005). Additionally, the linked cell algorithm lends itself readily to parallelization as described in Capecelatro and Desjardins (2013). Each processor is assigned a group of cells and therefore a subsection of the domain. Ghost cells are used at the processor boundaries to handle inter-processor interactions. The parallel algorithm is tested on case with $N_p = 40,000$ and shows linear scaling up to 32 processors. For a larger simulation with more particles, liner scaling to a larger number of processors is expected.

2.4. Initial conditions

In all of the simulations in this work, the desired initial condition is a fully packed and static bed of particles in a closed hopper. This allows the hopper to be opened at the start of the simulation and the particles then flow out of the hopper. However, generating a densely packed bed of particles directly is not a trivial problem. Instead, the particles are first initialized in a non-packed arrangement such as randomly placed in the domain or placed on a uniform lattice. Then, with a wall placed at the bottom of the hopper to close it, the particles are allowed to fall under the influence of gravity and settle to form the desired densely packed configuration. This process can be speed up by using larger than physical values for e and μ in order to quickly damp out the kinetic energy from the system (Pöschel and Schwager, 2005).

2.5. Periodic recycling of particles

This work is focused on studying the properties of steady state granular flows, where the statistics are stationary in time. This can be accomplished numerically by the use of periodic boundary conditions, allowing particles leaving the bottom of the domain to re-enter through the top. There has been numerical work where this has been done without any special treatment (Cleary and Sawley, 2002). However, in the present work, spurious fluctuations were observed caused by the re-entering particles impacting the top of the particle bed. Other work has used a technique where particles leaving were placed at the lowest location on the top of the particle bed with zero velocity (Hirshfeld et al., 1997). This allowed a level particle bed to be maintained while avoiding spurious effects caused by particles impacting with finite velocity. However, this technique is more difficult to implement and adds the expense of finding the correct location to place the particles.

In this work a technique is desired that allows the use of standard periodic boundary conditions while still avoiding spurious fluctuations. A new technique is developed where standard periodic boundary conditions are used in addition to a region where an artificial viscous force is added to the particles. The viscous force is chosen to be similar to an aerodynamic drag force

$$F_v \propto |\boldsymbol{v}_i| \boldsymbol{v}_i, \tag{18}$$

where the proportionality constant determines the terminal velocity of the particle. In the following cases, the constant is chosen such that the terminal velocity is approximately twice the mean velocity of the particles in the channel. This allows the re-entering particles to catch up to the particles in the channel, while slowing them down before impacting the top of the bed. This avoids spurious fluctuation velocities in the channel, while being very easy to implement and requiring minimal computational expense.

3. Model validation

Before using the DEM methodology described above to simulate the particle curtain in Wagner et al. (2012), the granular channel flow experiment in Natarajan et al. (1995) is used as a benchmark to validate the model.

3.1. Setup

The details of the experiment by Natarajan et al. are as follows. The dimensions of the channel are height $H=100$ cm, width $2W=5$ cm, and depth $d=2.18$ cm. The front and back walls are polished glass to replicate a 2-D flow. Two wall conditions are used for the side walls. A smooth wall condition is created using polished glass and a rough wall using particles glued to the walls in an approximately hexagonal close packed configuration. The particles are glass beads with a mean diameter of $D=3$ mm with a standard deviation of 2.13%. A feed hopper is used to feed particles into the channel. At the bottom of the channel is a flow control valve with variable width. This work will focus on the data obtained for a slit width of 1.3 cm.

Numerically, the setup shown in Fig. 1 is used. The width and depth of the domain are matched to the experiment. Instead of a feed hopper, periodic boundary conditions are used as described in Section 2.5 to create a steady flow of particles. The flow control valve geometry was not specified in the experiment, therefore a hopper design with angled walls is used where the angle α is determined as described in Section 3.2 below. Additionally, the 2.18% standard deviation in the particle diameter is matched numerically. A Gaussian distribution is chosen, however it is cutoff at two standard deviations to prevent small particles from overly restricting the time step and large particles from restricting the cell size for the linked-cell algorithm. Similar cutoffs have been used previously in numerical simulations (Cleary and Sawley, 2002).

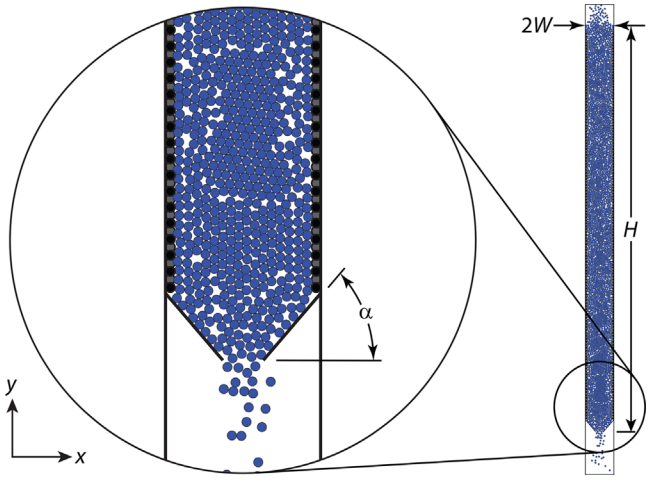

Fig. 1. Diagram showing the geometry of the DEM simulation of the vertical channel. The dimensions for the height H, half-width W, and hopper angle α are shown. The particles at the wall are fixed particles used to create a rough wall condition. In smooth wall cases, these are absent.

The polished glass walls are modeled as planes with the same properties as the glass particles. For the rough wall case, fixed particles are arranged in a hexagonal close packed arrangement at the wall.

The particle properties are chosen to match the properties of glass as used in the experiment. The specific type of glass used was not mentioned, however glass is known to have a density of 2400–2800 g/m^3. The value used in the simulation is determined as described in Section 3.2 below. The friction and restitution coefficients for binary collisions between small glass spheres have been measured as $e=0.97$ and $\mu=0.092$ (Foerster et al., 1994). Additionally, the elastic modulus is 60×10^9 Pa and Poisson's ratio is 0.24 (Gondret et al., 2002).

The coordinate system is shown in Fig. 1 with the y-axis pointing upward in the streamwise direction, x-axis in the transverse direction, and the z-direction along the depth of the channel. The $x=0$ location is the centerline of the channel. The velocity components in the x and y directions are u and v, respectively.

3.2. Model calibration

One parameter that is left to be determined is the height of channel H, and resulting N_p, that is required. It has been observed experimentally that, contrary to the behavior of a liquid, the pressure at the bottom of a hopper becomes independent of H above a critical height because the weight of the particles is supported by the sidewalls (Jaeger and Nagel, 1992). In testing what this critical height is, a simulation is performed where the periodic boundary conditions are not used, causing the particles to drain out of the hopper and not re-enter. Therefore H steadily decreases and the mass flow rate $\dot{m}$ is measured as a function of H. The simulations show that above $H\approx0.2$ m the mass flow rate becomes constant. In the final simulations, $H=0.75$ m is used, which is still small enough to compute in a reasonable time and is well above the critical height.

The next parameter that needs to be determined is the normal stiffness, k_n, for the spring model. If k_n is chosen to accurately match the elastic modulus of glass particles, the equations become impractically stiff and expensive to solve. For example, using the relation between k_n and the elastic modulus given in di Maio and di Renzo (2004) with a characteristic velocity of 1 m/s, $k_n=2.1\times10^6$ N/m would be required. In many cases it is possible to use a smaller k_n than would be needed to match the material properties, because the large scale flow features become independent of k_n in the limit of large k_n. A range of simulations are run at various k_n to determine when the solution properties of interest (mass flow rate $\dot{m}$, mean transverse and streamwise velocity components $\langle u\rangle$ and $\langle v\rangle$, and fluctuation transverse and streamwise velocity components u' and v') become independent of k_n. Here the angle brackets denote an averaged quantity, and the prime indicate the standard deviation. It is determined that all flow features of interest become independent of k_n at $k_n=1\times10^5$ N/m. Therefore $k_n=1\times10^5$ N/m is the value used in the remainder of the validation case simulations.

As mentioned in the previous section, the type of glass used for the particles (and therefore density ρ) and the angle α of the hopper walls is not specified in Natarajan et al. (1995). Therefore, these parameters are chosen as fitting parameters to match to the mass flow rate $\dot{m}$ and mean streamwise velocity $\langle v\rangle$ measured in the experiment. In order to determine the angle dependence of $\langle v\rangle$ (and $\dot{m}$ which is proportional to $\langle v\rangle$) on the hopper exit angle α, a number of cases were simulated with varying α. The results are plotted in Fig. 2. Experiments have shown empirically that

$$\dot{m}=A[\tan(90^\circ-\alpha)]^{-0.35}, \tag{19}$$

is a good fit to the dependence of $\dot{m}$ on α, where A is the constant of proportionality (Rose and Tanaka, 1959). This relation is only

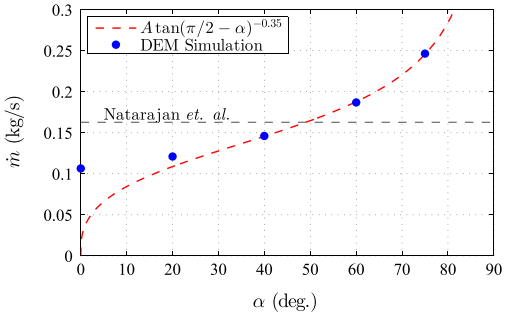

Fig. 2. Plot of $\dot{m}$ versus α. Data from this work are shown in filled symbols and the fitted empirical relation is the red dotted line. The horizontal dotted line is the experimentally measured $\dot{m}$.

Table 1
Physical properties of the particles used in the simulations.

Property	Symbol	Value	Units
Density	ρ	2600	kg/m^3
Poisson's ratio	ν	0.22	
Restitution coefficient	e	0.97	
Friction coefficient	μ	0.092	
Radius	R	1.5	mm
Normal stiffness	k_n	1×10^5	N/m

valid in the "mass flow" regime where there is no stagnant region near the hopper base, therefore it is only valid for $\alpha\gtrsim45^\circ$. The two largest α data points in Fig. 2 are fitted using least-squares by Eq (19) which yields $A=0.149$ kg/s and the resulting fit is plotted as a dashed line in Fig. 2. It is evident that the DEM predictions agree well for large α as is also observed by Anand et al. (2008) in a similar numerical experiment. By validating the angle dependence with the relation in Rose and Tanaka (1959), it allows interpolation to choose the correct α to match the conditions in Natarajan et al. (1995). Since it is observed that $\langle v\rangle$ is weakly dependent on ρ, and $\dot{m}\propto\langle v\rangle$, the hopper angle α is interpolated using Eq. (19) in order to match the $\langle v\rangle$ observed in Natarajan et al. (1995). Then, ρ is chosen in order to also match the $\dot{m}$ observed in the experiment. Using this process, the final ρ is 2600 kg/m^3 and the final α is determined to be 49.4°. Given the density range of glass given in the previous section, both these values are in the expected range.

The final properties of the particles used in the numerical simulations are given in Table 1.

3.3. Results

With ρ and α calibrated to match the experimentally measured $\dot{m}$ and $\langle v\rangle$, the simulation can be compared with the experimental measurements. The first step is computing the velocity profiles. In the experiment, the velocity of the particles are computed by tracking the displacement of a particle over images taken at a rate of 30 fps. The same technique was used to compute the velocity in the DEM simulations. In addition, the statistics of the velocity, such as the mean and standard deviation, need to be calculated as a function of location within the channel. In the experiment, bins were used and the velocities were averaged over all particles that pass through the bin. A particle is defined to be in the bin if its center is within the bin. Natarajan et al. (1995) used bins 0.5D wide by 2 cm high. It was found in the DEM results that using a bin 0.5D wide lead to bin-to-bin oscillations in the statistics due to the layering of particles near the boundary. In other work, bin sizes around 1.0D to 1.5D are often used (Moka and Nott, 2005; Gutfraind and Pouliquen, 1996; Alam and Chikkadi, 2010). Much smoother

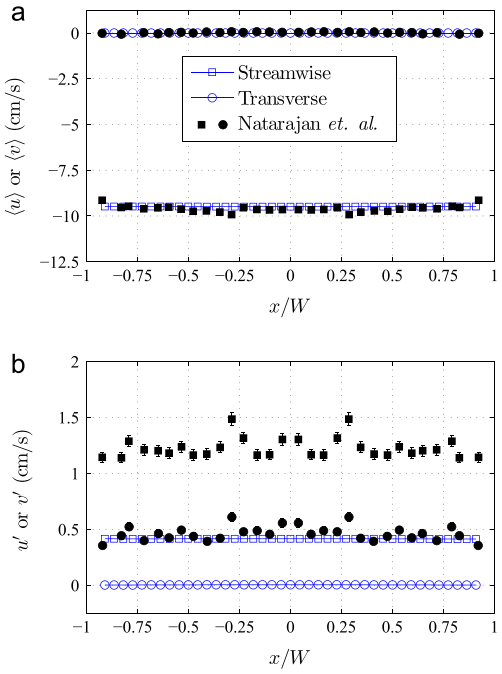

Fig. 3. Velocity profiles for the smooth-walled channel. Plots are included of (a) the mean velocity components $\langle u\rangle$ and $\langle v\rangle$ and (b) the fluctuating components u' and v'. Open symbols are data from this work and filled symbols are data from Natarajan et al. (1995). Squares are the streamwise component of velocity u and circles are the transverse component v.

statistics are obtained with bins 1.5D wide, therefore this is the size used in the plots below.

Simulations are performed for both smooth wall and rough wall cases. The smooth wall results are given in Fig. 3. Note that the data from Natarajan et al. was only reported for half of the channel. In the figures presented here, the data are mirrored about the channel centerline. The error bars on the fluctuating velocity components represent the 4% and 7% error in the streamwise and transverse components, respectively, as reported in Natarajan et al. (1995).

As seen in these results, a flat profile is correctly predicted, and the magnitude of the mean velocity in both the streamwise and transverse directions is correct. Looking at the results for the fluctuation velocity in Fig. 3b, it is apparent that in both the streamwise and transverse directions, the fluctuation magnitude is significantly under-predicted.

In the simulation of the rough walled channel, the calibration of α leads to a slightly different value of $\alpha=54.2^\circ$ in order to match the experimentally measured $\langle v\rangle$ at the centerline. The velocity profiles obtained for the rough wall case are plotted in Fig. 4. In Fig. 4a, the mean velocity profile shows good agreement with the experiment. The transverse component of the fluctuation velocity in Fig. 4b also shows reasonable agreement. However, some discrepancy between our simulation and the experimental data is observed in the streamwise fluctuation velocity. The fluctuations near the wall are correct, however the simulation is predicting much lower fluctuations in the center of the channel than was measured experimentally.

In the hope of obtaining results that more closely match the experiment, the friction and restitution coefficients are varied in order to see the dependence of the velocity profile on these quantities. As discussed in Appendix A below, varying these parameters did not yield improved agreement with the experimental data.

Another possible cause of the disagreement in the streamwise fluctuation is the simplified friction model in Eq. (16) that is being used as opposed to the full linear friction model in Eq. (12). We compared these two models by running both smooth and rough-

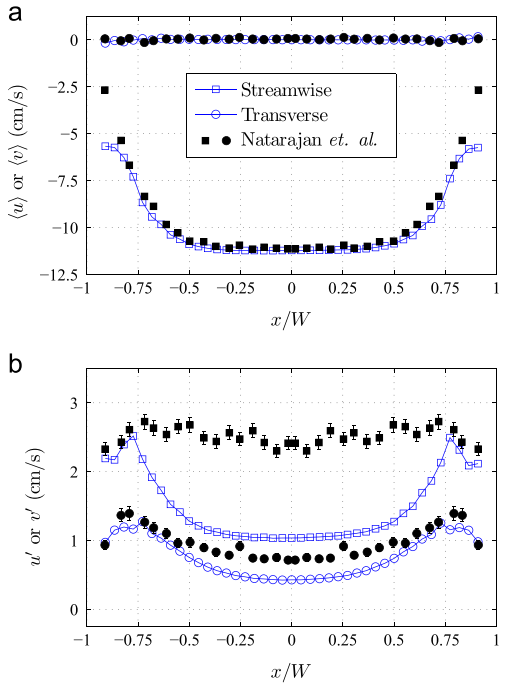

Fig. 4. Velocity profiles for the rough-walled channel. Plots are included of (a) the mean velocity components $\langle u \rangle$ and $\langle v \rangle$ and (b) the fluctuating components u' and v'. Open symbols are data from this work and filled symbols are data from Natarajan et al. (1995). Squares are the streamwise component of velocity u and circles are the transverse component v.

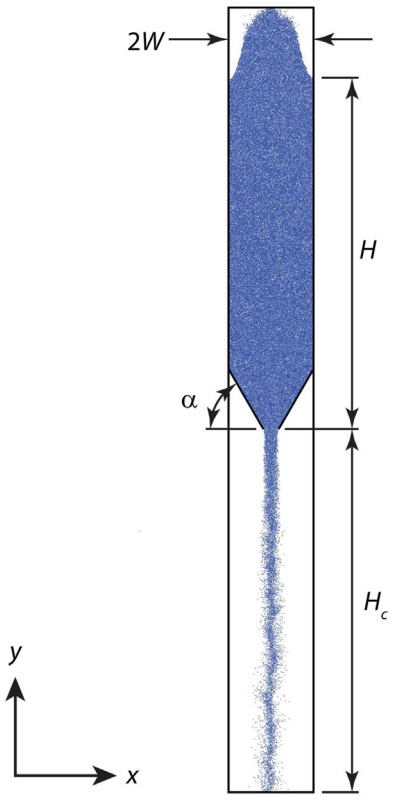

Fig. 5. Geometry of the numerical simulation of the particle curtain. The origin is at the center of the slit opening where the particle curtain begins.

walled channel cases using the open source DEM code LIGGGHTS (Kloss et al., 2012) using the same particle properties. The results are compared with the results from this work in Figs. 13 and 14 of Appendix A. For the smooth-walled channel, slightly better agreement is obtained for v', and in the rough-walled channel, slightly better results are obtained near the walls for $\langle v \rangle$ with the full linear model, however overall very similar results are obtained. These observations confirm those found in Capecelatro and Desjardins (2013) where they observed that the simplified model in Eq. (16) is a good compromise between accuracy and cost for granular flows dominated by sustained contact between particles.

Although, the shape of the $\langle v \rangle$ profile in Fig. 4 is very different from that obtained by Natarajan et al. other similar experimental work has yielded a qualitatively similar shape in fluctuation velocity. For example, Fig. 4d in MiDi (2004) shows a very similar profile with a peak in fluctuations near the walls and a minimum at the center of the channel, as opposed to the relatively flat profile obtained by Natarajan et al. The source of these qualitative differences is not clear. Overall, the results of the vertical channel flow validation show that with careful choice of model parameters, the DEM approach is useful for the prediction of the properties of granular flows with reasonable accuracy.

3.4. Periodic depth dependence

In the particle curtain that will be discussed next, the depth of the curtain in the z-direction (referring to the same coordinate system as the channel above) is large compared to its width. Therefore, numerically it can be considered semi-infinite and simulated using periodic boundary conditions on the z boundaries. However, it is unclear how large of depth d in the periodic direction needs to be simulated. Therefore, before the curtain is simulated, simulations of the vertical channel case at various d are performed. The steady-state mean and fluctuation velocities in the streamwise direction as well as the mass flow rate for the smooth-wall case are tracked as a function of d. It is observed that the mean velocity and mass flow rate are relatively independent of d, however the fluctuation velocity is not independent of d until $d = 10D$ where D is the mean particle diameter. In the next section, a depth of $10D$ is used when simulating the particle curtain.

4. Particle curtain predictions

Given the good agreement between our DEM simulations and the experimental results for the vertical channel flow, we proceed to simulate the particle curtain in Wagner et al. (2012). A discussion of the geometry and model parameters will be discussed next, followed by the results.

4.1. Setup

The geometry of the problem is shown in Fig. 5. The width of the hopper is $2W = 17.8$ mm and the slit opening is 3.2 mm wide. The walls at the bottom of the hopper are angled at $\alpha = 60^\circ$ with respect to horizontal. The visible length of the particle curtain is $H_c = 76.2$ mm and the particles are glass spheres with diameters sorted to 106–125 μm. For a full description of the experiment, see Wagner et al. (2012).

The particle diameters are chosen to have a Gaussian distribution with a mean of 115.5 μm and standard deviation of 4.75 μm. The distribution was cut off at two standard deviations to give the correct diameter bounds of 106 μm and 125 μm. From the channel flow simulations it is determined that for a height above $4(2W)$, the mass flow rate becomes independent of height. Therefore, the height of particles in the feed hopper is chosen such that $H \geq 71.2$ mm for this particle curtain simulation. The depth in the periodic z-direction must be $d \geq 10D$ for the solution properties to be independent of d as determined in Section 3.4. Using the mean

particle diameter, this requires $d=1.155$ mm. All particle properties except for k_n (which is discussed below) are the same as those used in the channel flow simulation given in Table 1 above because glass particles are being simulated in both cases.

For post-processing the statistics of the particle curtain, the same bin-wise averaging as above is used. In this case, the bin dimensions are chosen to be $2D$ by $10D$ in the x and y directions, respectively. In calculating the solid volume fraction of a bin, the total volume of the spheres whose centers lie in the bin is divided by the total bin volume. This value is then time averaged. The errors associated with particles overlapping the edges of the bin are averaged out through the time averaging process.

4.2. Results

The above geometry requires approximately 1.5 million particles to be simulated. The high computational cost and limited resources demand that the time step size (determined by N) and spring stiffness k_n be chosen judiciously to satisfy accuracy of the solution and computational cost. Simulations are first performed at various N. It is found that by using $N=15$, the error is estimated to be less than 5% for all relevant quantities. Additionally, varying N has no significant effect on the qualitative behavior of the particle curtain. The stiffness k_n was chosen to be 32 N/m as this is the largest that could be simulated given the resources available. Any errors associated with simulating overly soft particles is discussed following the presentation of the results.

The averaged solid volume fraction β profiles at various y locations are shown in Fig. 6. It is evident that immediately after the particles leave the slit opening, β is a nearly uniform 60% across the width of the curtain. The theoretical maximum β for spheres of equal sizes is 74.05%, and the random close packing limit has been observed to be 60–68% (Torquato et al., 2000).

By the time the particles reach $y=-19.3$ mm, the relatively flat β profile has become Gaussian-like. As the particles continue to fall further from the slit opening, the evolution of the β profile is mostly characterized by the dilation due to the gravitational acceleration. At the midpoint of the curtain ($y=-38.1$ mm) the volume fraction at the centerline is 43% and the curtain is approximately 4 mm wide. The wording in Wagner et al. (2012) suggests a relatively uniform β across the width of the curtain. Although this is observed immediately after the particles exit the curtain, for the bulk of the curtain a highly non-uniform, Gaussian-like, profile is observed in this work.

A look at the mean velocity profiles for the $\langle u\rangle$ and $\langle v\rangle$ velocity components in Fig. 7a and b, respectively, explain the behavior of β. At the top of the curtain, there is a very thin region where the $\langle u\rangle$ velocity points inward caused by the angled side walls that form the slit opening. This inward velocity causes the β profile to be pushed toward the center and become nonuniform. Below this region, there is a wide portion of $\langle u\rangle\approx 0$ in the center of the curtain with the outer edges having velocities pointing outward. This

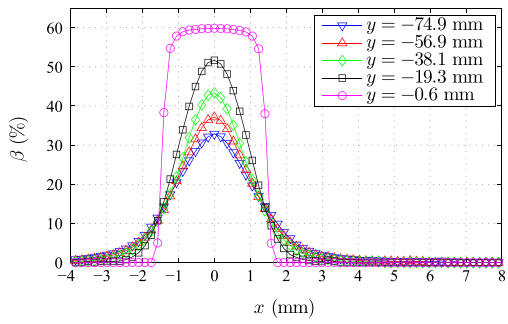

Fig. 6. Volume fraction β versus x at various y locations in the particle curtain.

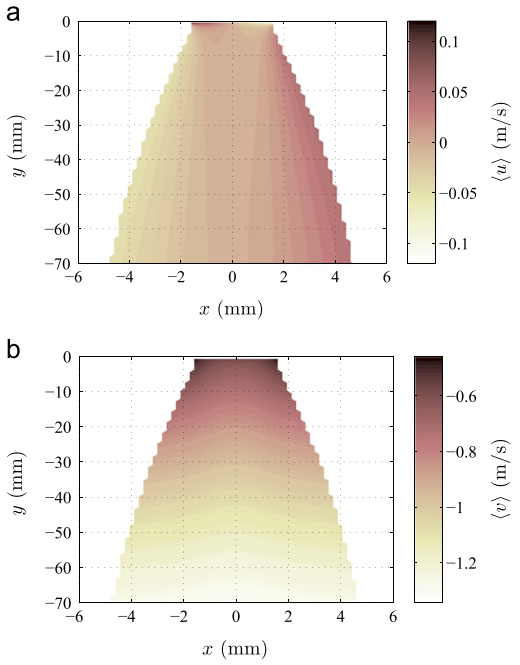

Fig. 7. Contour plot of (a) the horizontal component of the mean velocity $\langle u\rangle$ and (b) the vertical component of the mean velocity $\langle v\rangle$.

explains the relatively constant shape of the β profiles observed everywhere outside the thin region at the top of the curtain. Note that these velocity contours are only shown on the bins that have at least 10 particles to average over.

Additionally, it is interesting to look at the contour plots of the fluctuation velocities u' and v' in Fig. 8a and b, respectively. In both plots, there is a very thin region near the hopper exit where there are relatively large fluctuation velocities. However, outside of this region the fluctuations are small. This explains the lack of "diffusion-like" spreading of the β profile.

However, comparison with the data from Wagner et al. (2012) reveals some striking discrepancies. The experiment estimated $\beta=21\pm 2\%$ and observed a curtain width of 2 mm at the midpoint of the curtain. In Fig. 6, the data at $y=-38.1$ mm predict a much wider curtain and β at the center more than double the experimentally observed estimate. Additionally, private communication with the corresponding author of Wagner et al. (2012) revealed that the numerically simulated mass flow rate is approximately double what is observed experimentally. It is believed that these discrepancies are caused by the overly soft nature of the particles in the simulation.

In order to assess the impact of using a small particle stiffness, simulations using even smaller values of k_n are shown in Fig. 9. Note that these data are taken at $y=-38.1$ mm and are simulated for a narrower domain of $d=3D$. These data reveal that as k_n is increased, the predicted particle curtain becomes narrower. If the particles were the correct stiffness, one could reasonably expect the simulated curtain to be closer to the 2 mm width that is observed experimentally.

4.3. Soft particle effects

The effect of overly soft particles on the magnitude of the flow quantities can be tested by revisiting the channel flow simulation discussed in Section 3. For this smaller validation case, using $k_n=1\times 10^5$ N/m and $N=50$ results in accurate predictions of the flow. However, if $N=15$ is used and k_n is decreased, the effect on the simulated results can be observed and possibly extended to this larger particle curtain simulation.

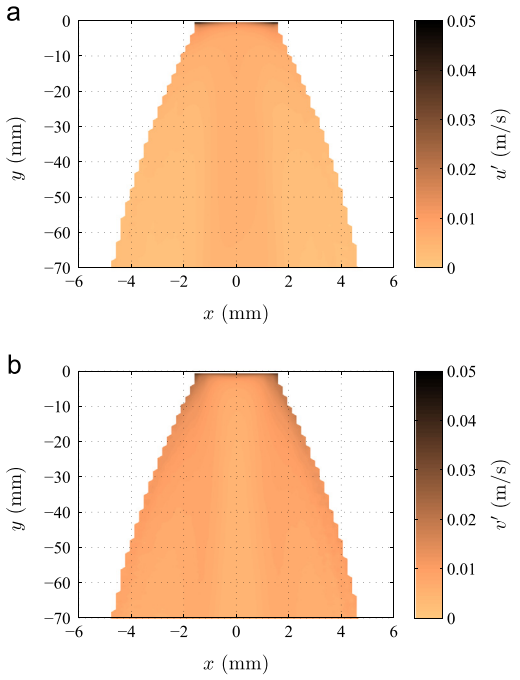

Fig. 8. Contour plot of (a) the horizontal component of the fluctuation velocity u' and (b) the vertical component of the fluctuation velocity v'.

Starting with the same material properties and geometry as used in the final results presented in Section 3.3, α was changed to 60° in order to match α that is used in the particle curtain. A baseline, fully-resolved, case is run with $k_n = 1 \times 10^5$ N/m and $N=50$. Then N is changed to 15 and k_n is decreased holding all other parameters constant in order to replicate the same level of under-resolution and particle softness that is present in the particle curtain case. The percent error of the steady mass flow rate $\dot{m}$, average streamwise velocity $\langle v \rangle$, and volume fraction β immediately below the hopper exit are shown in Fig. 10. Note that for all quantities, a positive error signifies that the quantity has a larger magnitude than the accurate case using $k_n = 1 \times 10^5$ N/m and $N=50$.

As seen in Fig. 10, by choosing a low k_n it is possible to get a $\dot{m}$ that is nearly double the properly resolved case. Additionally, β and $\langle v \rangle$ are also 38% and 27% over-predicted, respectively in the case with the softest particles. Interestingly, although not presented here, $\beta = 60\%$ at the hopper exit for the softest-particle case, which is nearly the same as predicted in the particle curtain case in Fig. 6. This also agrees with the fact that an accurate prediction of β at the hopper exit should be less than the random close packing limit of 60–68% because of the dilation that is required for movement. These results give some indication that the particles in the curtain simulation are significantly softer than necessary for quantitative predictions.

If we assume that similar error magnitudes are present in the particle curtain case, namely 38% and 27% too large for β and $\langle v \rangle$, respectively, we can apply a correction to the volume fraction profiles in Fig. 6. The dilation effect caused by the gravitational acceleration is accounted for by assuming free-fall acceleration of the particles. The scaled data are shown in Fig. 11. The scaled data show that β at $y = -38.1$ mm has the potential to be much lower than the current simulation with overly-soft particles indicates, and the average may in fact be similar to $\beta = 21 \pm 2\%$ that is cited in Wagner et al. (2012) if the correct stiffness is used.

Despite the errors caused by overly soft particles in the simulations that limit the quantitative accuracy of this data, the qualitative trends are not expected to change if the correct stiffness were used.

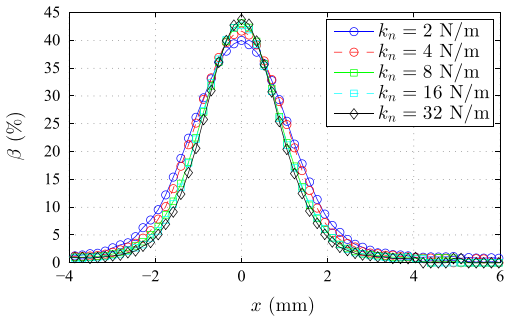

Fig. 9. Volume fraction β versus x at $y = -38.1$ mm for various k_n.

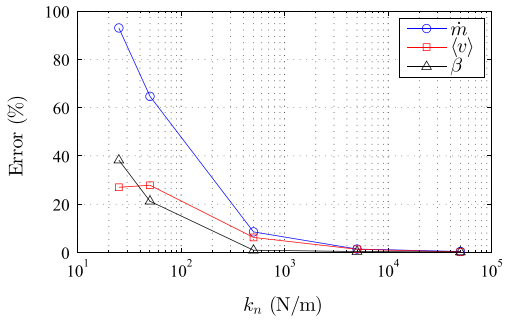

Fig. 10. Percent error in $\dot{m}$, $\langle v \rangle$, and β versus k_n for the channel flow case discussed in Section 3 above. All results are for $N=15$ and the error is calculated based on a simulation with $k_n = 1 \times 10^5$ N/m and $N=50$. A positive error indicates the magnitude is larger than in the fully-resolved case.

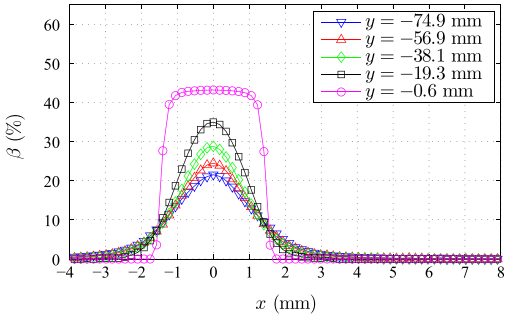

Fig. 11. Volume fraction β versus x at various y locations in the particle curtain. These data are scaled to the expected values if β and $\langle v \rangle$ at the hopper exit in the simulated results are 38% and 27% too large, respectively.

Therefore, the results presented above still provide valuable insight into the properties of the particle curtain in Wagner et al. (2012).

5. Summary and conclusions

The goal of this work is to better understand the properties of the particle curtain in Wagner et al. (2012). To simulate the granular flow from a feed hopper through a slit opening, the discrete element method is used. The linear-spring and dashpot model is used for the normal component of the collisional force and a static friction model is used for the tangential component. In order to simulate a steady flow of particles through the domain, periodic boundary conditions are used in conjunction with a novel damping force that slows re-entering particles to avoid spurious fluctuation velocities.

To validate our DEM model, we first simulate a granular channel flow and compare with the experimental results in Natarajan et al. (1995). The profiles of the mean and fluctuating components of both the streamwise and transverse velocity components within

the channel are compared. Both smooth and rough wall conditions are tested. In both cases, the mean velocity show excellent agreement with the experiment. The smooth wall case under-predicts both components of the fluctuation velocity. However, in the rough-wall case, the transverse fluctuation velocity is well predicted. The streamwise fluctuation velocity in the rough wall case shows some disagreement in the center of the channel, but qualitatively agrees with the results from similar experiments.

Finally, the properties of the particle curtain in Wagner et al. (2012) are examined. Contrary to indications from the experimental results, the DEM simulations show a Gaussian-like volume fraction profile across the width of the curtain. The behavior of the particle curtain is governed mostly by free-fall. The fluctuation velocities are mostly confined to the region near the hopper exit and are observed to quickly decay as the particles fall.

Comparison with the data in Wagner et al. (2012) indicates that the DEM results have error believed to be caused by the simulated particles being overly soft. Error analysis suggests that results using a larger stiffness would show better agreement with the curtain width, volume fraction, and mass flow rate that are observed experimentally. This also highlights the importance of modeling particles with adequate stiffness to produce quantitative flow predictions.

Acknowledgments

The research reported in this paper is partially supported by the HPC equipment purchased through: NSF MRI (Grant no. CNS 1229081); NSF CRI (Grant no. 1205413).

Appendix A. Effect of collision model and parameters

In the hope of improving the quality of agreement between the experimental and DEM results in the channel flow simulation, the friction coefficient μ and restitution coefficient e are adjusted. μ is tested in the range 0.00–0.15 and e from 0.9 to 1.0. All results are for the rough-walled channel case. Note that these results are simulated with the hopper angle $\alpha = 49.4^\circ$ calibrated for the smooth-wall case, as opposed to the recalibrated $\alpha = 54.2^\circ$ that is presented for the rough-walled channel in the main text.

It is evident in Fig. 12 that changing μ has the most pronounced effect on the mean streamwise velocity $\langle v \rangle$. With decreasing μ there is an increase in $\langle v \rangle$. This is in agreement with intuition, as less friction allows particles to slide past each other more easily and therefore flow through the channel more quickly. Additionally, with decreasing μ, it is observed that u' at the channel walls increases. However, none of the results obtain a better overall result when compared to the experimentally measured values.

Changing e has a negligible effect on the velocity profiles, therefore varying this parameter did not yield a better result.

Another parameter that is worth investigating is the choice of friction model. In this work, the simplified model in Eq. (16) is used as a compromise between accuracy and computational cost. However, it is interesting to see the effect of using the more accurate full linear friction model in Eq. (12). To preform this comparison, the open source code LIGGGHTS (Kloss et al., 2012) is used to simulate both the rough and smooth walled channel cases. In LIGGGHTS, the full linear friction model is used, but all other model parameters are kept fixed. The comparison between the LIGGGHTS results and those from this work are presented in Figs. 13 and 14 for the smooth and rough walled channels, respectively.

It is observed that for the smooth walled channel, v' is closer to the measured value in the experiment when using the full linear friction model. However, v' remains under-predicted in both cases.

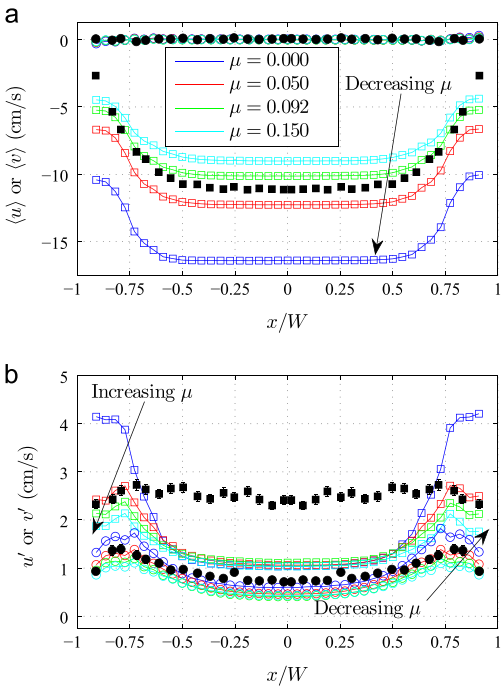

Fig. 12. Velocity profiles for the rough-walled channel simulated at various μ. Plots are included of (a) the mean velocity components $\langle u \rangle$ and $\langle v \rangle$ and (b) the fluctuating components u' and v'. Open symbols are data from this work and filled symbols are data from Natarajan et al. (1995). Squares are the streamwise component of velocity u and circles are the transverse component v.

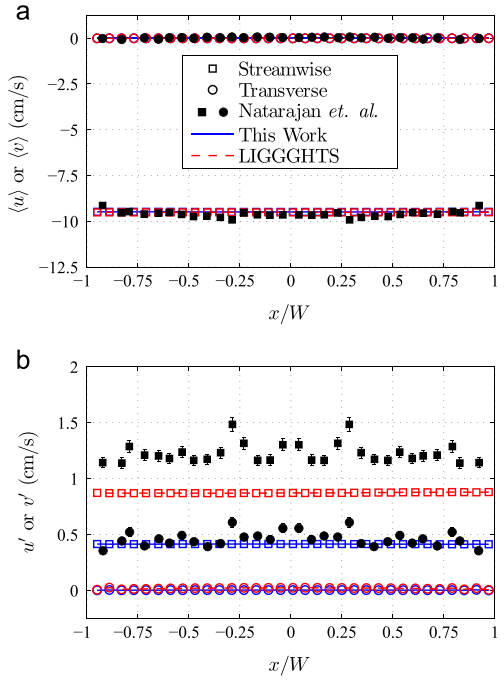

Fig. 13. Comparison of the results from this work and LIGGGHTS for the smooth-walled channel. Plots are included of (a) the mean velocity components $\langle u \rangle$ and $\langle v \rangle$ and (b) the fluctuating components u' and v'. Open symbols are data from this work and filled symbols are data from Natarajan et al. (1995). Squares are the streamwise component of velocity u and circles are the transverse component v.

The only other significant difference between the two friction models is $\langle v \rangle$ at the wall of the rough-walled channel. Slightly better agreement is observed using the full linear friction model. In general, both models produce roughly equivalent results, however

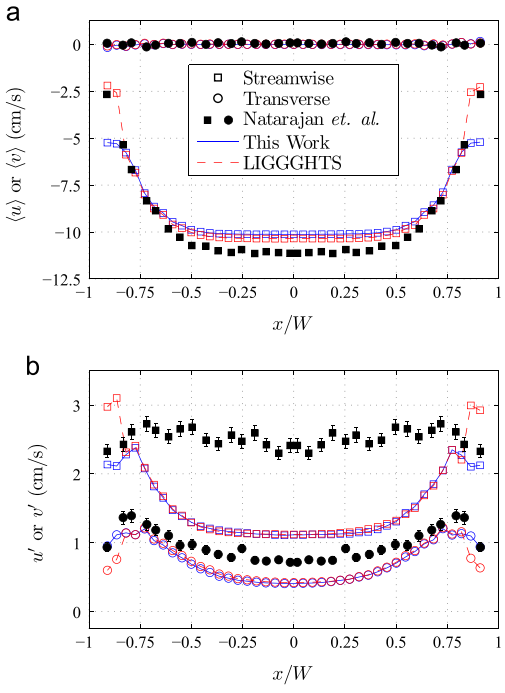

Fig. 14. Comparison of the results from this work and LIGGGHTS for the rough-walled channel. Plots are included of (a) the mean velocity components $\langle u \rangle$ and $\langle v \rangle$ and (b) the fluctuating components u' and v'. Open symbols are data from this work and filled symbols are data from Natarajan et al. (1995). Squares are the streamwise component of velocity u and circles are the transverse component v.

the full linear model requires additional computational expense and memory.

References

Alam, M., Chikkadi, V.K., 2010. Velocity distribution function and correlations in a granular Poiseuille flow. J. Fluid Mech. 653, 175–219.

Anand, A., Curtis, J.S., Wassgren, C.R., Hancock, B.C., Ketterhagen, W.R., 2008. Predicting discharge dynamics from a rectangular hopper using the discrete element method (DEM). Chem. Eng. Sci. 63, 5821–5830.

Baer, M.R., Nunziato, J.W., 1986. A two-phase mixture theory for the deflagration-to-detonation transition (DDT) in reactive granular materials. Int. J. Multiph. Flow 12, 861–889.

Capecelatro, J., Desjardins, O., 2013. An Euler–Lagrange strategy for simulating particle-laden flows. J. Comput. Phys. 238, 1–31.

Choi, J., Kudrolli, A., Rosales, R.R., Bazant, M.Z., 2004. Diffusion and mixing in gravity-driven dense granular flows. Phys. Rev. Lett. 92, 174301.

Cleary, P.W., Sawley, M.L., 2002. DEM modelling of industrial granular flows: 3D case studies and the effect of particle shape on hopper discharge. Appl. Math. Model. 26, 89–111.

Crowe, C.T., Schwarzkopf, J.D., Sommerfeld, M., Tsuji, Y., 2012. Multiphase Flows with Droplets and Particles, Second edition CRC Press, New York.

Cundall, P.A., Strack, O.D.L., 1979. A discrete numerical model for granular assemblies. Géotechnique 29, 47–65.

Deen, N.G., van Sint Annaland, M., van der Hoef, M.A., Kuipers, J.A.M., 2007. Review of discrete particle modeling of fluidized beds. Chem. Eng. Sci. 62, 28–44.

di Maio, F.P., di Renzo, A., 2004. Analytical solution for the problem of frictional-elastic collisions of spherical particles using the linear model. Chem. Eng. Sci. 59, 3461–3475.

Drew, D.A., 1983. Mathematical modeling of two-phase flow. Annu. Rev. Fluid Mech. 15, 261–291.

Foerster, S.F., Louge, M.Y., Chang, H., Allia, K., 1994. Measurements of the collision properties of small spheres. Phys. Fluids 6, 1108.

Gondret, P., Lance, M., Petit, L., 2002. Bouncing motion of spherical particles in fluids. Phys. Fluids 14, 643.

Gutfraind, R., Pouliquen, O., 1996. Study of the origin of shear zones in quasi-static vertical chute flows by using discrete particle simulations. Mech. Mater. 24, 273–285.

Hirshfeld, D., Radzyner, Y., Rapaport, D.C., 1997. Molecular dynamics studies of granular flow through an aperture. Phys. Rev. E 56, 4404–4415.

van der Hoef, M.A., Ye, M., van Sint Annaland, M., Andrews, A., Sundaresan, S., Kuipers, J.A.M., 2006. Multiscale modeling of gas-fluidized beds. Adv. Chem. Eng. 31, 65–149.

Hu, G., Hu, Z., Jian, B., Liu, L., Wan, H., 2011. On the determination of the damping coefficient of non-linear spring-dashpot system to model hertz contact for simulation by discrete element method. J. Comput. 6, 984–988.

Jaeger, H.M., Nagel, S.R., 1992. Physics of the granular state. Science 255, 1523–1531.

Jop, P., Forterre, Y., Pouliquen, O., 2006. A constitutive law for dense granular flows. Nature 441, 727–730.

Ketterhagen, W.R., Curtis, J.S., Wassgren, C.R., Kong, A., Narayan, P.J., Hancock, B.C., 2007. Granular segregation in discharging cylindrical hoppers: a discrete element and experimental study. Chem. Eng. Sci. 62, 6423–6439.

Kloss, C., Goniva, C., Hager, A., Amberger, S., Pirker, S., 2012. Models, algorithms and validation for opensource DEM and CFD-DEM. Prog. Comput. Fluid Dyn. 12, 140–152.

Li, J., Goniva, P.A., Webb, C., Dyakowski, T., 2004. Flow of sphero-disc particles in rectangular hoppers—a DEM and experimental comparison in 3D. Chem. Eng. Sci. 59, 5917–5929.

Magnaudet, J., Eames, I., 2000. The motion of high-Reynolds-number bubbles in inhomogeneous flows. Annu. Rev. Fluid Mech. 32, 659–708.

MiDi, G.D.R., 2004. On dense granular flows. Eur. Phys. J. E 14, 341–365.

Moka, S., Nott, P.R., 2005. Statistics of particle velocities in dense granular flows. Phys. Rev. Lett. 95, 068003.

Natarajan, V.V.R., Hunt, M.L., Taylor, E.D., 1995. Local measurements of velocity fluctuations and diffusion coefficients for a granular material flow. J. Fluid Mech. 304, 1–25.

Pöschel, T., Schwager, T., 2005. Computational Granular Dynamics: Models and Algorithms. Springer, Berlin, The Netherlands.

Olivier, Pouliquen, François, Chevoir, 2002. Dense flows of dry granular material. C. R. Phys. 3, 163–175.

Powers, J.M., Stewart, D.S., Krier, H., 1990. Theory of two-phase detonation—Part I: modeling. Combust. Flame 80, 264–279.

Regele, J.D., Rabinovitch, J., Colonius, T., Blanquart, G., 2014. Unsteady effects in dense, high speed, particle laden flows. Int. J. Multiph. Flow 61, 1–13.

Rose, H.E., Tanaka, T., 1959. Rate of discharge of granular materials from bins and hoppers. Engineer 208, 465–469.

Savage, S.B., 1979. Gravity flow of cohesionless granular materials in chutes and channels. J. Fluid Mech. 92, 53–96.

Sielamowicz, J., Dippel, S., Wolf, D.E, 1996. Force schemes in simulations of granular materials. J. Phys. I 6, 5–20.

Sielamowicz, I., Bloñski, S., Kowalewski, T.A., 2006. Digital particle image velocimetry (DPIV) technique in measurements of granular material flows, Part 2 of 3-converging hoppers. Chem. Eng. Sci. 61, 5307–5317.

Torquato, S., Truskett, T.M., Debenedetti, P.G., 2000. Is random close packing of spheres well defined? Phys. Rev. Lett. 84, 2064–2067.

Wagner, J.L., Beresh, S.J., Kearney, S.P., Trott, W.M., Castaneda, J.N., Pruett, B.O., Baer, M.R., 2012. A multiphase shock tube for shock wave interactions with dense particle fields. Exp. Fluids 52, 1507–1517.

Zhu, H.P., Zhou, Z.Y., Yang, R.Y., Yu, A.B., 2008. Discrete particle simulation of particulate systems: a review of major applications and findings. Chem. Eng. Sci. 63, 5728–5770.